Photodissociation of Azulene at 193 nm: Ab Initio and RRKM Study

Yu. A. Dyakov,*,† C.-K. Ni,†,‡ S. H. Lin,†,§ Y. T. Lee,†,§ and A. M. Mebel⊥

Institute of Atomic and Molecular Sciences, Academia Sinica, P.O. Box 23-166, Taipei 10764, Taiwan, Department of Chemistry, National Tsing Hua University, Hsinchu, Taiwan, Chemistry Department, National Taiwan University, Taipei, Taiwan, and Department of Chemistry and Biochemistry, Florida International University, 11200 SW 8th Street, Miami, Florida 33199

Received: June 15, 2005; In Final Form: July 28, 2005

The ab initio/Rice−Ramsperger−Kassel−Marcus (RRKM) approach has been applied to investigate the photodissociation mechanism of azulene at 6.4 eV (the laser wavelength of 193 nm) upon absorption of one UV photon followed by internal conversion into the ground electronic state. Reaction pathways leading to various decomposition products have been mapped out at the G3(MP2,CC)//B3LYP level and then the RRKM and microcanonical variational transition state theories have been applied to compute rate constants for individual reaction steps. Relative product yields (branching ratios) for the dissociation products have been calculated using the steady-state approach. The results show that photoexcited azulene can readily isomerize to naphthalene and the major dissociation channel is elimination of an H-atom from naphthalene. The branching ratio of this channel decreases with an increase of the photon energy. Acetylene elimination is the second probable reaction channel and its branching ratio rises as the photon energy increases. The main C_8H_6 fragments at 193 nm are phenylacetylene and pentalene and the yield of the latter grows fast with the increasing excitation energy.

Introduction

Polycyclic aromatic hydrocarbons (PAHs) are known to be major air pollutants resulting from incomplete combustion of fossil fuels and also, together with their cations, have been proposed as possible carriers of the unidentified infrared emission bands from various interstellar objects.[1,2] As the simplest PAHs, azulene and naphthalene (Chart 1) have been intensively investigated in recent decades both experimentally and theoretically. One of the major subjects of these studies is the transformation of azulene to naphthalene. The thermal rearrangement from azulene to naphthalene in the gas phase has been studied in numerous experiments using the ^{13}C-labeling technique.[3−15] Several intramolecular reaction mechanisms have been proposed[8,16−20] to explain carbon permutations observed in the experiments. However, none of these mechanisms alone can explain all experimental data. DFT and ab initio calculations at the B3LYP/6-31G* and MP2/6-311+G(3df,2p) levels performed by Alder et al.[21] showed that the preferable reaction mechanism for this reaction in the gas phase is a radical promoted mechanism, which initiates by the formation of $C_{10}H_7$ and $C_{10}H_9$ radical intermediates and provides several alternative ways of rearrangement. They obtained a barrier of 39.2 kcal/mol for the spiran pathway and 43.6 kcal/mol for the methylene walk pathway, which is at least 30 kcal/mol lower than the values calculated for the closed-shell system. Later, Parrinello and co-workers employed the Car−Parrinello metadynamics method to compare the intramolecular and radical-promoted pathways.[22] They concluded the norcaradiene pathway to be the preferable intramolecular mechanism with barrier heights of 81.5−98.6 kcal/mol, whereas the radical routes have activation energies of 24−39 kcal/mol.

CHART 1

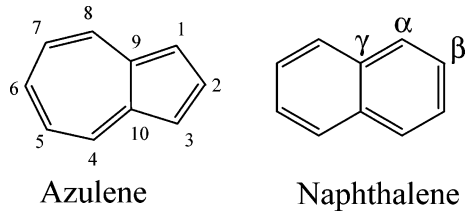

Azulene Naphthalene

Photoreactions of azulene and naphthalene cation radicals were studied experimentally and theoretically by several research groups. For instance, Jochims et al.[23,24] investigated photofragmentation of naphthalene and azulene and deuterium isotope effects on the photofragmentation thresholds of naphthalene monocations in the energy range of 7−22 eV. They also performed semiempirical MNDO calculations of the azulene−naphthalene isomerization reaction and gave a complete outline of all possible photofragmentation reactions that could be observed in this energy range. Lifshitz and co-workers investigated photoisomerization and photodissociation of the naphthalene and azulene cations[25−29] using time-dependent photoionization mass spectrometry (TPIMS). They established that, being excited, the azulene cation rearranges into naphthalene with a barrier of approximately 80 kcal/mol, and then dissociates to $C_{10}H_7^+$ and $C_8H_6^+$ fragments with similar branching ratios. The type of $C_8H_6^+$ cation was not established from the experiment. Additional attempts were performed to determine the configuration of the $C_8H_6^+$ fragment. Schroeter et al.[30] investigated mass spectra of several types of $C_8H_6^+$ and concluded that the $C_8H_6^+$ fragment should be a benzocyclobutadiene cation. Van der Hart,[31] on the basis of DFT B3LYP/cc-pVDZ calculations of naphthalene dissociation channels,

† Academia Sinica.
‡ National Tsing Hua University.
§ National Taiwan University.
⊥ Florida International University.

10.1021/jp053218m CCC: $30.25
Published on Web 09/08/2005

concluded that both phenylacetylene and benzocyclobutadiene cations could be observed in photodissociation experiments.

Experiments with neutral azulene and naphthalene revealed that most of the excited azulene nonradiatively relaxes to the vibrationally excited ground state due to ultrafast internal conversion, and the internal conversion rate remains fast with an increase of the excess energy.[32−34] This allows one to prepare highly vibrationally excited azulene and naphthalene molecules in the ground electronic state and investigate their isomerization and dissociation behavior. Experiments with azulene in a molecular beam using the multimass ion imaging techniques under 193 nm photoexcitation performed by Ni's group[35] indicated that vibrationally excited azulene isomerizes to naphthalene with a rate of 4.1×10^5 s^{-1}, and then eventually dissociates through the H-atom elimination channel with a rate of 5.1×10^4 s^{-1}. The most recent molecular beam experiments of this research group on azulene photodissociation[36] reveal a minor acetylene elimination channel in addition to the H-atom elimination. The initial stage of acetylene elimination has not been resolved due to the small probability of this channel. Kinetic energy distribution of acetylene and C_8H_6 fragments shows a maximum at 20−25 kcal/mol. In most cases, the maximum in kinetic energy distribution is closely related to the difference between the energy of the exit barrier and energies of products (the reverse barrier height from the products).

To clarify the azulene−naphthalene rearrangement mechanism under molecular beam collisionless conditions and explain the acetylene elimination mechanism, accurate ab initio calculations of the potential energy surface (PES) are necessary. The MP2 calculations, which were already reported[21] for this system, may not be sufficient to describe the kinetics of the azulene photodissociation reaction with high accuracy. Therefore, in this paper we revisit previous semiempirical and DFT calculations following the azulene−naphthalene rearrangement schemes proposed earlier,[8,16−22] and calculate rate constants and branching ratios of main isomerization and dissociation channels using the RRKM statistical approach.

Computational Methods

The geometries for all intermediates and transition states were fully optimized using the hybrid density functional B3LYP method[37,38] with the 6-31G* basis set.[39] Connections between transition states and corresponding local minima were confirmed by intrinsic reaction coordinate (IRC) calculations. Optimized geometries of various intermediates and transition states and their total energies are given in the Supporting Information. Energies of intermediates and transition states at B3LYP/6-31G* optimized geometries were calculated using the G3-type computational scheme,[40a] in particular, its G3(MP2,CC)//B3LYP modification.[40b,c] Zero point energy (ZPE) corrections were taken into account using B3LYP/6-31G* frequencies without scaling. All calculations were performed employing the GAUSSIAN 98[41] and MOLPRO 2002[42] packages. Rice−Ramsperger−Kassel−Marcus (RRKM) and microcanonical variational transition state theories[43−45] have been applied to compute rate constants for individual reaction steps. G3 energies and B3LYP/6-31G* frequencies for all intermediates and transition states were used to perform the RRKM calculations. In these calculations, available internal energy was taken to be equal to the energy of a 193 nm photon absorbed by the azulene molecule (148.1 kcal/mol). Relative product yields (branching ratios) were found using the steady-state approach. For the radical product channels, C_8H_7 + H, no distinct transition states exist on the PES for the last reaction step, as it is a simple bond cleavage process. In this case, we used the variational transition state theory (VTST)[45] by considering different positions for the transition state along the reaction path, calculating rate constants corresponding to each of them, and finding the minimal rate. To perform VTST calculations, the B3LYP/6-31G* energies were scaled by the ratio of energies of the products calculated at the B3LYP/6-31G* and G3 levels. Before the scaling, the basis correction term, i.e., the difference between MP2/G3MP2large and MP2/6-31G* energies, was subtracted from the G3 energies of products. These terms were calculated exactly along the H-atom elimination potential energy profile and then added to the scaled B3LYP/6-31G* energies. Additional computational details of our ab initio/RRKM/VTST approach have been described earlier.[46]

In the section devoted to a discussion on the most favorable pathways of azulene−naphthalene isomerization, we were interested first in a qualitative comparison of rate constants for all discussed pathways. Since preliminary estimates reveal great distinction in rate constants for different pathways and omission of several intermediates separated by low barriers could not distort the qualitative reaction scheme, only the highest in energy transition states along each route were used as barriers between azulene and naphthalene to compute rate constants for particular pathways. Nevertheless, for the final calculations of phodissociation product branching ratios and the overall rate constant we used a more sophisticated reaction scheme including most important intermediates and the steady-state approximation was employed.

Results and Discussion

I. Azulene−Naphthalene Rearrangement. Earlier theoretical investigations of azulene and naphthalene revealed a great variety of routes for the azulene−naphthalene isomerization. Roughly, all possible reaction mechanisms can be divided into six main groups. These are (1) CH-group transfer from the seven-member ring to the five-member ring of azulene through a bicyclobutane-like structure (bicyclobutane mechanism), first proposed by Scott et al.,[4] (2) azulene → naphthalene rearrangement through a norcaradiene-like structure followed by a hydrogen shift (norcaradiene−vinylidene, or Dewar−Becker mechanism, originally proposed by Becker et al.[8] and Dewar et al.[19]), (3) cleavage of the 9,10-bond in azulene, first proposed by Scott et al.,[9] (4) migration of a CH_2-group from the seven-member ring of azulene to the five-member ring (methylene group migration, first proposed by Alder et al.[5]), (5) hydrogen shift followed by one-step rearrangement to naphthalene (originally proposed by Alder et al.[5−7]), and (6) a spiran pathway. The isomerization through a spiro structure, discussed earlier,[5−7,16,19] was established to play an important role in the radical-promoted mechanism.[21] In this paper, we explore this mechanism for neutral azulene.

1. Bicyclobutane Mechanism. The bicyclobutane isomerization mechanism (Figure 1) initiates from rearrangement of the seven-member ring of azulene into a benzvalene-like structure of intermediate **Is3** through a barrier at **TS1**, followed by the CH-group transfer from the benzvalene-like structure toward the five-member ring above a barrier at **TS2**, and formation of the bicyclobutane-like intermediate **Is4**. In turn, **Is4** rearranges to a metastable minimum **Is5**, which then isomerizes to the naphthalene. The highest transition state along this route is **TS1** with a barrier height of 80.2 kcal/mol. Rate constants corresponding to **TS1** are 1.9×10^4 s^{-1} in the forward direction and 9.6×10^1 s^{-1} in the reverse direction. This rearrangement mechanism has been studied earlier by Alder et al.[21] at the MP2/

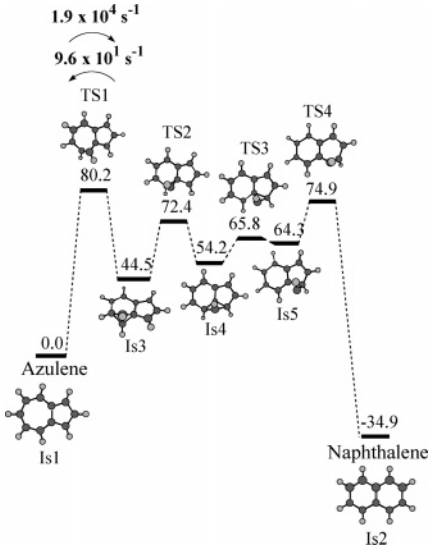

Figure 1. Bicyclobutane mechanism of azulene-to-naphthalene isomerization.

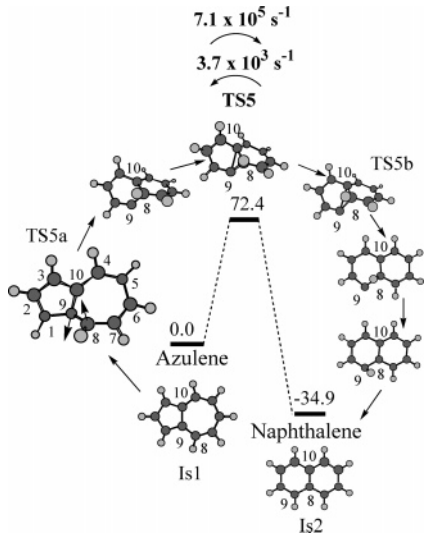

Figure 2. Norcaradiene mechanism of azulene-to-naphthalene isomerization.

6-311+G(3df,2p) level. They obtained for the highest barrier along this pathway the value of 86.2 kcal/mol.

2. Norcaradiene−Vinylidene Mechanism. The norcaradiene−vinylidene mechanism is a one-step azulene−naphthalene rearrangement with a barrier of 72.4 kcal/mol (Figure 2). The process initiates from a simultaneous decrease of the distance between the carbon atoms 8 and 10 and an increase of the distance between atoms 9 and 10 (see structure **TS5a** on the minimal energy reaction path obtained by IRC calculations, Figure 2). As a result, in the transition state configuration (**TS5**) the molecule has the five- and six-member rings joined by a triangle consisting of the carbon atoms 8, 9, and 10. The hydrogen atom linked to the carbon atom 8 of azulene still keeps this connection in the transition state. After going over the transition state, the distance between atoms 9 and 10 increases and the molecule, by passing via a vinylidene-like structure **TS5b**, attains a planar structure with two six-member rings. At the same time, the hydrogen atom initially bound to the atom 8 shifts toward the atom 9, finally leading to the naphthalene structure. This reaction mechanism is very similar to the Dewar−Becker mechanism, computed for the azulene cation radical by Koster et al.[28] at the CCSD/cc-pVDZ level, and is

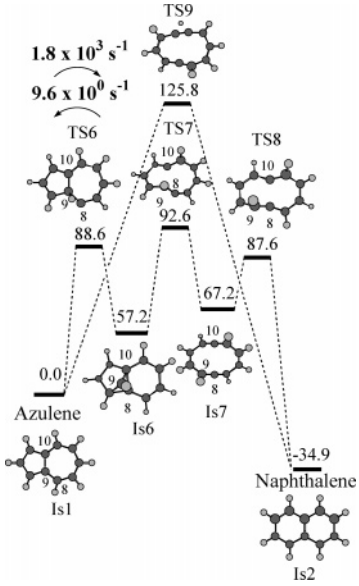

Figure 3. 9,10-Bond cleavage mechanism of azulene-to-naphthalene isomerization.

proposed to be the major isomerization route. For the cation radical system, an additional intermediate, hydrogen shifted naphthalene, separates the ring's distortion and the hydrogen shift rearrangement stages. For the neutral system, rate constants of the azulene−naphthalene isomerization through the norcaradiene−vinylidene mechanism are 7.1×10^5 and 3.7×10^3 s^{-1} in the forward and reverse directions, respectively. This rearrangement mechanism has been studied earlier by Alder et al.[21] at the MP2/6-311+G(3df,2p) level who obtained for the highest barrier along this pathway the value of 79.6 kcal/mol.

3. Cleavage of the 9,10-Bond. There are two possible pathways of the direct azulene 9,10-bond cleavage (Figure 3). The first is a one-step 9,10-bond cleavage with simultaneous H-shift (**TS9**). The corresponding transition state has a ten-member-ring structure. The barrier along this route is extremely high (125.8 kcal/mol). The second pathway initiates from a hydrogen shift between positions 8 and 9 in azulene. The hydrogen-shifted azulene resulting from this step and established as a minimum by the B3LYP/6-31G* geometry optimization is not a minimum at the G3 computational level. This metastable intermediate relaxes to a norcaradiene-like structure **Is6** without a barrier. The geometry of **Is6** differs from the geometry of the norcaradiene-like structure **TS5** by the position of one hydrogen atom. At the **Is6** geometry, the hydrogen atom is located near the ninth carbon, whereas in **TS5** the hydrogen is positioned near the carbon 8. The intermediate **Is6** rearranges to a ten-member-ring intermediate **Is7** after overcoming a barrier of 92.6 kcal/mol at **TS7**. Then, **Is7** isomerizes to naphthalene by ring closure through a transition state **TS8**. The critical transition state on this pathway is **TS7**. Rate constants corresponding to **TS7** are 1.8×10^3 and 9.6×10^3 s^{-1} in the forward and reverse directions, respectively.

4. Methylene Walk. Isomerization of azulene into naphthalene through a CH_2-group migration starts from a hydrogen shift between the carbon positions 4 and 5 (Figure 4). Both directions of the shift are possible, so there are two alternative routes at the initial stage of the methylene walk pathway: through **TS10** and **TS12** with barrier heights of 85.4 and 88.8 kcal/mol, respectively. Both routes eventually converge through several metastable structures to the same intermediate **Is11**, which has two fused six- and five-member rings with an out-of-ring CH_2 group. At the next step, the CH_2 group bound to the six-member

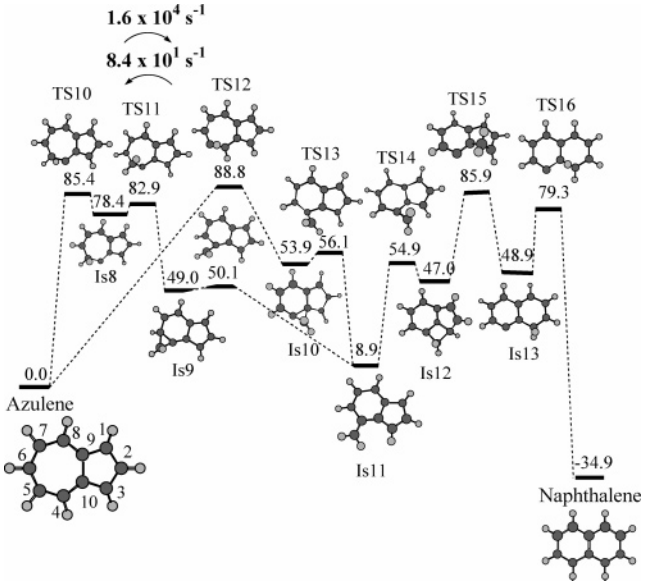

Figure 4. Methylene walk mechanism of azulene-to-naphthalene isomerization.

ring transfers toward the five-member ring over the barriers at **TS14** and **TS15** producing the structures **Is12** and then **Is13**, which finally isomerizes to naphthalene by an inter-ring hydrogen shift. In this scheme, we have omitted some intermediates that were found to be local minima after B3LYP/6-31G* geometry optimization, but not minima at the G3 computational level.

According to this scheme, there are three barriers, at **TS10**, **TS12**, and **TS15**, that should be tested as the limiting stage for the methylene walk pathway. RRKM calculations performed within an assumption of a single transition state along the pathway give values of 1.3×10^4, 3.1×10^3, and 7.0×10^4 s^{-1} in the forward direction, and 6.8×10^1, 1.6×10^1, and 3.7×10^1 s^{-1} in the reverse direction. Taking into account that **TS10** and **TS12** provide alternative routes on the first stage of the pathway and the rate constants for **TS15** are significantly higher than those for **TS10** and **TS12**, we conclude that the barriers at **TS10** and **TS12** are the limiting stages of the pathway and find the resultant rate constants as a sum of those for **TS10** and **TS12**, which gives 1.6×10^4 s^{-1} in the forward direction. However, in the reverse direction the reaction step going over **TS15** is critical and the rate constant can be estimated as 3.7×10^1 s^{-1}.

5. Hydrogen Shift. The hydrogen shift mechanism is similar to the norcaradiene−vinylidene channel described above. The main difference is that the hydrogen shift precedes rearrangement of the rings (Figure 5). The first step on this route is isomerization of azulene to the **Is6** intermediate through **TS6**, which is similar to the 9,10-bond cleavage mechanism. The next step is rearrangement of the norcaradiene structure **Is6** to naphthalene through the transition state **TS17**. The rate-limiting stage of this pathway is the hydrogen shift with a barrier of 88.6 kcal/mol at **TS6**. Rate constants, corresponding to this transition state, are 4.0×10^3 and 2.2×10^1 s^{-1} in the forward and reverse direction, respectively.

This reaction mechanism is very similar to the corresponding azulene cation radical rearrangement mechanism, calculated at the CCSD/cc-pVDZ level[28] and proposed as one of preferable pathways of the azulene−naphthalene isomerization reaction.

6. Spiro-Radical Mechanism. This pathway starts from rearrangement of azulene into a spiro structure **Is14**, which has the electronic wave function of a biradical open-shell singlet character (Figure 6). Due to a multideterminant character of

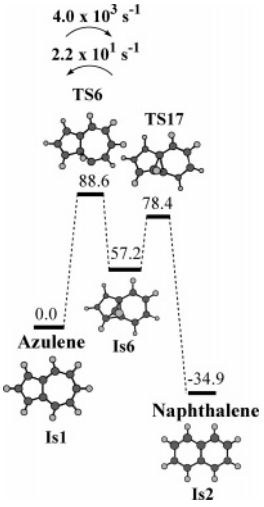

Figure 5. Hydrogen shift mechanism of azulene-to-naphthalene isomerization.

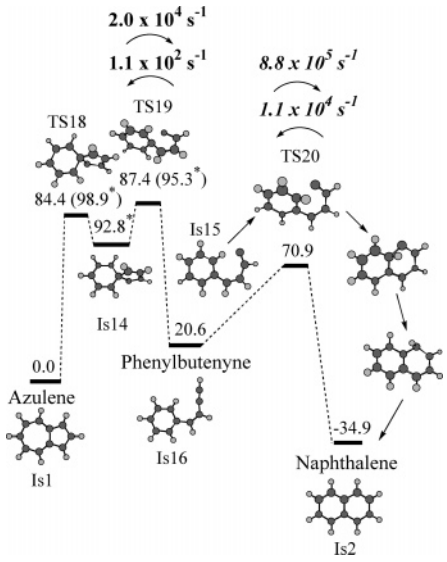

Figure 6. Spiro-radical pathway of azulene-to-naphthalene isomerization. Italic numbers above TS20 show the rate constants for the phenylbutenyne-to-naphthalene isomerization. Energies denoted with an asterisk were calculated at the UB3LYP/6-31G* level.

the wave function, it is impossible to use the G3 computational level to calculate energy of the spiro-intermediate **Is14**. In this case, the UB3LYP/6-31G* energies instead of G3 energies were presented. The next step is rearrangement of the spiro-structure to a methastable *cis*-vinylidene intermediate **Is15** through the transition state **TS19**, and then isomerization to the phenylbutenyne **Is16**. B3LYP/6-31G* geometry optimization revealed a small (3.2 kcal/mol) barrier between **Is15** and **Is16**, but G3 energy calculations confirmed that **Is15** is not a local minimum. The configuration of **TS19** was found employing UB3LYP/6-31G* geometry optimization for an open-shell singlet state starting from a triplet wave function. Because of the instability of the wave function in the vicinity of **TS19**, we were not able to confirm the connection of **TS19** with **Is14** and **Is15** by IRC calculations. Nevertheless, UB3LYP/6-31G* geometry optimization of the singlet electronic state starting from this vicinity with a triplet initial guess for the wave function converged to either **Is14** or **Is15**. Phenylbutenyne isomerizes to naphthalene through transition state **TS20** having a vinylidene structure. The energy of the barrier (70.9 kcal/mol) and the transition state structure are very close to the energy and geometry of **TS5** for

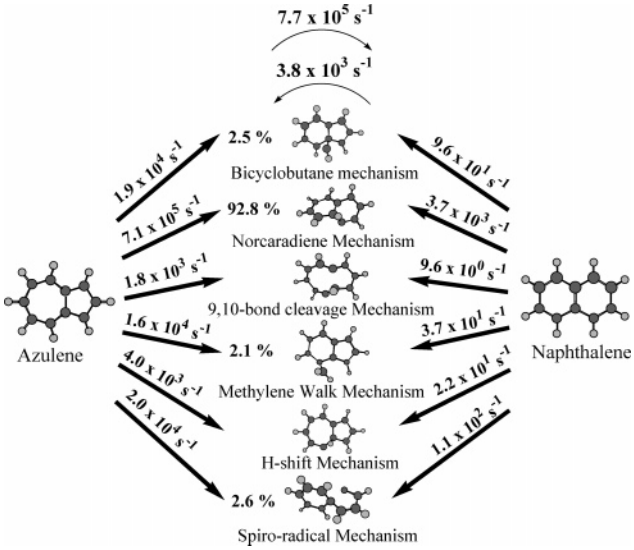

Figure 7. Generalized scheme of azulene-to-naphthalene rearrangement.

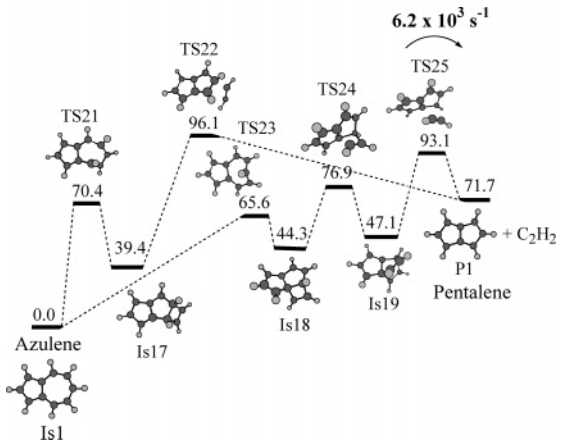

Figure 8. Acetylene elimination pathways starting directly from azulene.

the norcaradiene−vinylidene pathway. The critical transition state along the spiro-radical pathway is **TS19**, lying 87.4 kcal/mol above azulene. The rate constants corresponding to **TS19** are 2.0×10^4 and 1.1×10^2 s^{-1} in the forward and reverse directions, respectively.

The scheme in Figure 7 summarizes the discussion on the azulene−naphthalene isomerization mechanism. According to this scheme, the major rearrangement channel is the norcaradiene−vinylidene pathway that provides 92.8% of naphthalene. The bicyclobutane, methylene walk, and spiro-radical pathways give 2.5%, 2.1%, and 2.6% of the product, respectively. The total rate constants of azulene−naphthalene isomerization reaction are 7.7×10^5 and 3.8×10^3 s^{-1} in the forward and reverse direction, respectively, which is in good agreement with the experimental value of 4.1×10^5 s^{-1} for the forward direction obtained in the molecular beam experiment.[35] This confirms the validity of the suggested reaction scheme and sufficient accuracy of energy calculations performed in this work.

II. Azulene and Naphthalene Dissociation. *1. C_2H_2 Elimination.* A scheme of acetylene elimination from azulene is presented in Figure 8. There are two possible pathways of this reaction: the first goes through **Is17** and the second passes through **Is18**. In both intermediates, the seven-member ring rearranges into two fused five- and four-member rings, but they are oriented differently with respect to the pentacycle of azulene.

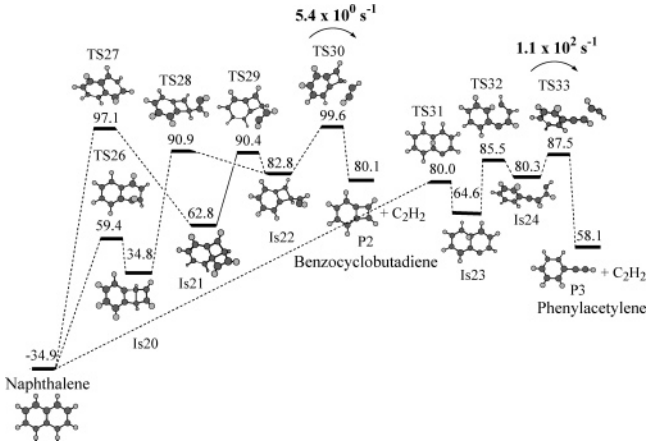

Figure 9. Acetylene elimination reactions from naphthalene. Photodissociation initiates from photoexcitation of azulene.

The final product for both routes is pentalene, C_8H_6, as the acetylene molecule is eliminated from the four-member ring in the intermediates. The highest barriers along the first and second routes are 96.1 and 93.1 kcal/mol, respectively. The differences between the barriers at the highest transition state and the energy of the products (reverse barriers) are 24.4 and 21.4 kcal/mol for the first and the second routes, respectively. These values are related to the maximum of the kinetic energy distribution observed in experiment.[36] Judging from the calculated reverse barriers, these pathways can be considered as possible candidates for the acetylene elimination channel. If one excludes metastable intermediates from this pathway and defines the highest transition state as the limiting stage on the route, the total rate constant of the C_2H_2 loss process has a value of 6.2×10^3 s^{-1}.

Figure 9 shows possible acetylene elimination channels from naphthalene. Here we suppose that naphthalene itself has been produced from vibrationally excited azulene. Two different C_8H_6 isomers can be formed from naphthalene. The first reaction pathway is the benzocyclobutadiene channel. It features the formation of Dewar-benzene-like intermediates **Is20** or **Is21**, where two fused four-member rings are oriented differently with respect to the remaining six-member cycle, followed by the C_2H_2 loss. The highest barrier for this channel is calculated for the last reaction step (**TS29**) and is 99.6 kcal/mol (relative to azulene), which is higher than that for acetylene elimination from azulene, 93.1 kcal/mol. The rate constant obtained within an assumption that the highest transition state is the limiting stage on this route is 5.4×10^0 s^{-1}, which is 3 orders of magnitude lower than that for the C_2H_2 loss from azulene. This makes this dissociation channel unfavorable in comparison to the pentalene channel. Meanwhile, the reverse barrier for this route is approximately 20 kcal/mol, making it a possible candidate for the elimination channel observed experimentally.

The second pathway is the phenylacetylene channel. It proceeds first by a hydrogen shift to one of the carbons involved in the C−C bond fusing two aromatic rings of naphthalene (**Is23**), which is followed by ring opening to **Is24**, and is completed by C_2H_2 elimination from the out-of-ring hydrocarbon chain. The highest barrier along this route is 87.5 kcal/mol at **TS33** for the last reaction step, which is 12 kcal/mol lower than that for the benzocyclobutadiene channel. However, the reverse barrier for this pathway is about 30 kcal/mol, which is significantly larger than the maximum observed on the experimental kinetic energy distribution curve. Employing the same approximate method for the rate constant calculation as for the previous C_2H_2 elimination routes, the rate constant for this pathway is 1.1×10^2 s^{-1}.

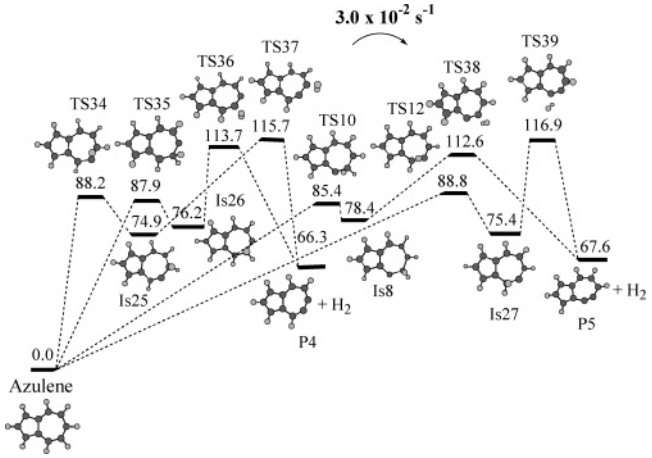

Figure 10. H_2 loss reactions from azulene.

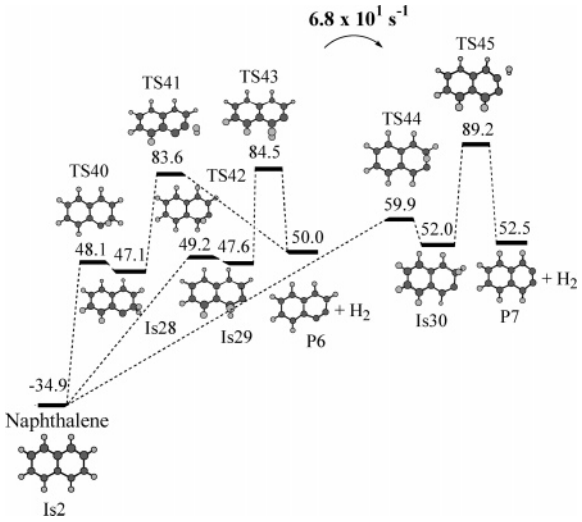

Figure 11. H_2 loss reactions from naphthalene. Photodissociation starts from photoexcitation of azulene.

2. H_2 Elimination. Figures10 and 11 present H_2 loss processes from azulene and naphthalene, respectively. In all cases, the reaction initiates by a hydrogen shift to a neighboring position and is followed by H_2 elimination. H_2 eliminations from other hydrogen shifted naphthalene isomers that could be obtained by consequent H migrations have barriers of approximately 10 kcal/mol higher than the elimination from single-hydrogen-shifted isomers (**Is28**−**Is30**) and therefore are neglected. The barriers for the elimination from azulene are much higher than those from naphthalene (112.6 kcal/mol for azulene vs 83.6 kcal/mol for naphthalene). For the rate constant calculations, only the highest transition states were taken into account. The total rate constant for the four possible H_2 eliminations from azulene (Figure 10) is 3.0×10^{-2} s^{-1}, which is extremely low in comparison with fast azulene−naphthalene rearrangement and other elimination channels. The total rate constant of H_2 loss processes from naphthalene (Figure 11) has a value of 6.8×10^1 s^{-1} that is comparable with rate constants for the acetylene elimination reaction.

3. H-Atom Elimination. H-atom elimination processes from azulene and naphthalene can be realized by two different mechanisms. The first mechanism is a direct C−H bond cleavage without distinct transition states (Figure 12). Rate constants in this case were found by using the variational transition state theory. The total rate constants for hydrogen elimination from azulene and naphthalene are 1.8×10^0 and 1.1×10^4 s^{-1}, respectively. Thus, H-atom loss is much more likely from naphthalene than from azulene.

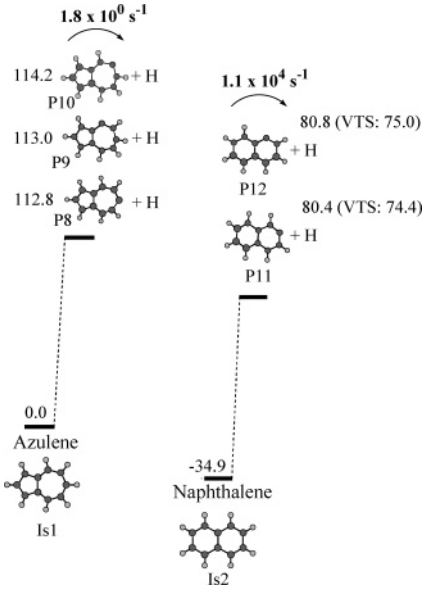

Figure 12. H-atom elimination from azulene and naphthalene.

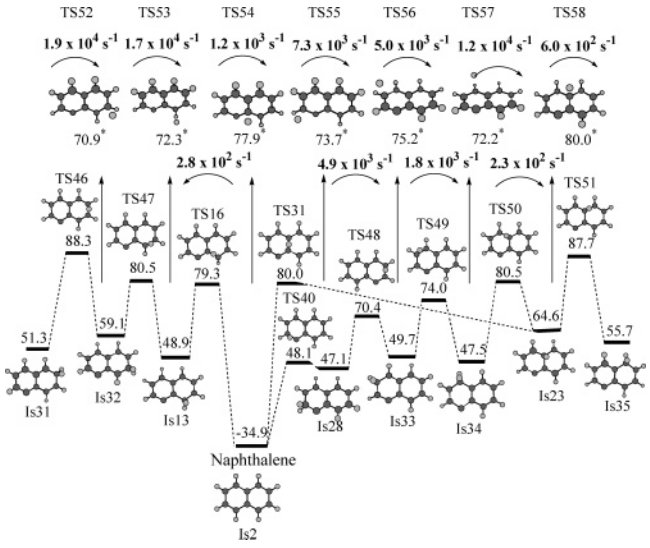

Figure 13. H-atom elimination through the hydrogen shift mechanism. Energies denoted with an asterisk were calculated at the UB3LYP/6-31G* level and then scaled by the ratio of energies of the products calculated at the B3LYP/6-31G* and G3 levels (as described in the text).

The second mechanism initiates by hydrogen shifts and is followed by H-atom elimination from CH_2 groups. Figures 13 and 14 present the reactions starting from the α and β positions of naphthalene. Geometries of H-atom elimination transition states were found by the UB3LYP/6-31G* geometry optimization of open-shell singlet states starting from a triplet wave function. All H-atom elimination routes, being started from H-shifted naphthalene and calculated at the UB3LYP/6-31G* level, exhibit small exit barriers. Taking into account that the B3LYP/6-31G* energies significantly differ from the G3 energies for hydrogen shifted naphthalenes and its dissociation products, we tried to calculate the G3 energy for all hydrogen elimination transition states. Unfortunately, we could not perform CCSD(T) calculations for these transition states due to a multideterminant character of wave functions. Instead, we employed the same procedure as for the direct H-atom elimination and scaled the UB3LYP/6-31G* energies by the ratio of

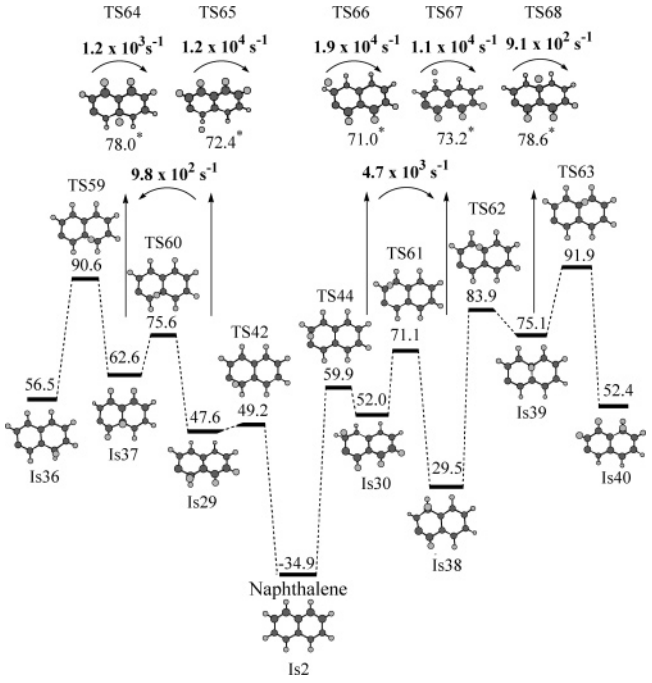

Figure 14. H-atom elimination through the hydrogen shift mechanism (continued).

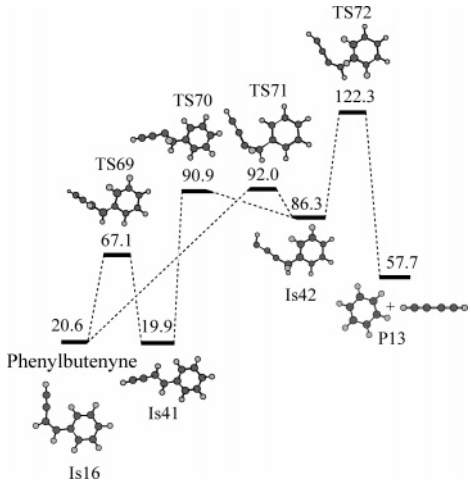

Figure 15. C_4H_2 elimination channels.

energies of the products calculated at the B3LYP/6-31G* and G3 levels. Before scaling, the basis correction term, i.e., the difference between MP2/G3MP2large and MP2/6-31G* energies, was subtracted from the G3 energies of products. These terms were calculated exactly for all the transition states and then added to the scaled UB3LYP/6-31G* energies. The described simplified calculations decrease the transition state energies to values that are lower than the energy of the products. In Figures 13 and 14, these energies are denoted with asterisks. Nevertheless, the structures of the transition states found at the UB3LYP/6-31G* level appeared to correspond to the minimal rate constants calculated along the corresponding H-atom elimination potential energy profiles.

Migrations of hydrogen atoms along the six-member rings and H-atom loss processes have comparable magnitudes of rate constants. So, the overall rate constant for each elimination channel is determined by the minimal rate constant among these two processes. The results presented in Figures 13 and 14 show that only the first and the second hydrogen shifts could influence the reaction rate for H elimination. The other elimination routes seem to be unlikely due to relatively low rate constants for the corresponding hydrogen shift reactions. All reaction rates shown in Figures 13 and 14 are calculated within an assumption that only the highest transition states along each route determine the rate constants. Preliminary tests performed for several reaction routes revealed a good agreement of multistep rate constants with those obtained by the simplified one-step scheme. The total rate constant computed for the H-atom elimination reaction through the hydrogen shift mechanism is 5.0×10^4 s^{-1}, so about 80% of H atoms eliminate through the hydrogen shift mechanism. This result seems to be surprising, as intuitively the reverse reaction of H addition to a radical site of the naphthyl radical should be faster than that to a CH group. Therefore, H elimination from a CH group could be expected to be faster than that from a CH_2 group. If we consider the corresponding rate constants excluding reaction path degeneracies (symmetry factors), indeed, the values for the H loss directly from CH groups are normally higher than those from CH_2 groups. On the other hand, the overall reaction path degeneracy for H elimination from CH_2 groups, 96, is more than an order of magnitude higher than the total symmetry factor for the direct H loss from CH, 8. In addition, due to the use of the approximate scheme for the energy evaluation (see above) of transition states for H loss from CH_2, the corresponding rate constants and the branching ratios of H loss from CH_2 can be somewhat overestimated. We did not take into account azulene H-atom elimination reactions through the hydrogen shift mechanism because the rate constants should be at least not higher than those for the direct H-atom elimination, which are negligible.

4. C_4H_2 Elimination. The last dissociation channel that is worth mentioning in this paper is the fragmentation to benzene and C_4H_2. This reaction path initiates from the azulene rearrangement to phenylbutenyne **Is16** (Figure 6) and is followed by hydrogen migrations through barriers at **TS69** and **TS70** leading to *trans*- and *cis*-phenylbutenyne, respectively (Figure 15). The hydrogen shifted phenylbutenyne intermediate **Is42** then loses a hydrogen eventually in favor of the phenyl residue via the barriers at **TS72** and **TS74**, and finally, yields $C_6H_6 + C_4H_2$. The highest barrier on this reaction path at **TS72** is 122.3 kcal/mol, which is too high to observe these products experimentally at the excitation energy of 6.4 eV. Hence, we do not include this reaction channel to the final reaction scheme.

III. Overall Reaction Scheme, Steady-State Rate Constants, and Branching Ratios. The overall reaction scheme is shown in Figure 16. Here, we extend the previous approximate calculation schemes by an addition of some important intermediate steps and include the azulene-to-naphthalene rearrangement process into consideration. Calculations display that the major dissociation channel is H-atom elimination (99%), which occurs after isomerization of azulene to naphthalene. This result is in good agreement with the molecular beam experiment for azulene.[35] The next important group of reaction channels includes decompositions into the C_2H_2 and C_8H_6 fragments. Two possible kinds of C_8H_6 fragments can be observed in experiments. The first is pentalene (0.7%), which is formed directly from the azulene molecule without isomerization to naphthalene. The second is phenylacetylene (0.2%), which is produced after the rearrangement to naphthalene. The benzocyclobutadiene fragment (less than 0.01%) is predicted to have too low yield to be observed in the molecular beam experiment. Clearly, the $C_8H_6 + C_2H_2$ products are relatively minor as compared to $C_{10}H_7 + H$. Although the rate constants for the individual reaction steps leading to these products shown in Figure 16 are seemingly large, for example, in the range of 10^6-10^8 s^{-1} for the formation of pentalene, one needs to remember that in a

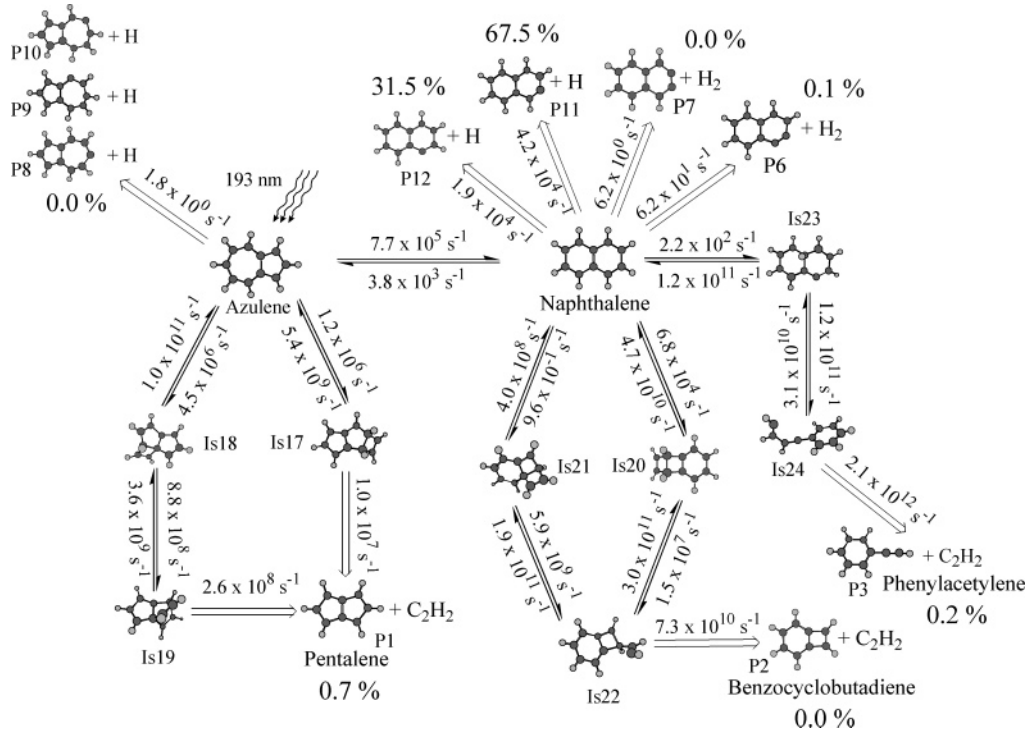

Figure 16. The overall reaction scheme of azulene photodissociation.

multistep reaction the overall rate constant is also determined by the steady-state concentration of intermediates on the reaction pathway. In the case of pentalene, such steady-state concentrations are computed to be very low, 2.2×10^{-4}, 4.4×10^{-5}, and 1.0×10^{-5} for **Is17**, **Is18**, and **Is19**, respectively, in fractions of the azulene concentration. As a result, the steady-state rate constants for the formation of pentalene are 2.2×10^3 s^{-1} via **Is17** and 2.6×10^3 s^{-1} via **Is18** and **Is19**. The overall rate constant for the production of pentalene directly from azulene (without taking into account the isomerization of azulene to naphthalene and backward) is then 4.8×10^3 s^{-1}, slightly lower than the value of 6.2×10^3 s^{-1} obtained previously without taking the existence of the intermediates into account. H_2 elimination is the third possible dissociation product that can be observed and the branching ratio of this channel is 0.1%.

The calculated value of the total rate constant of azulene photodissociation is 6.1×10^4 s^{-1}, which is in good agreement with the experimental value of 5.1×10^4 s^{-1}.[35] The results of the RRKM calculation using the steady-state approximation for multistep reactions refine the preliminary estimates of the rate constants presented in the previous sections and also allow us to evaluate the product branching ratios much more accurately. The $C_{10}H_7 + H$ products clearly dominate the photodissociation reaction, but it is also interesting to see relative branching ratios of the minor $C_8H_6 + C_2H_2$ and $C_{10}H_6 + H_2$ products. Initially, we obtained rate constants of 6.2×10^3, 1.1×10^2, and 6.8×10^1 s^{-1} for the pentalene, phenylacetylene, and $C_{10}H_6$ elimination channels, respectively, which, if used directly, give the relative branching ratios of 56:1:0.6 for the pentalene, phenylacetylene, and $C_{10}H_6$ products. However, from the steady-state calculations we obtained the relative branching ratios as 3.5:1:0.6 (the absolute branching ratios of these products approximately are only 0.7%, 0.2%, and 0.1%, respectively). The reason for the difference in the results is that the reactions pass through at least two sequential steps. The first one is the azulene-to-naphthalene isomerization that competes with the acetylene elimination process leading to pentalene. The second step is dissociation of naphthalene to phenylacetylene + C_2H_2, benzocyclobutadiene + C_2H_2, or $C_{10}H_6 + H_2$, and reverse rearrangement to azulene followed by decomposition to pentalene + acetylene. The reverse rearrangement rate constant is twice as low as the rate constant for pentalene elimination from azulene. Therefore, the rate-limiting stage for the pentalene channel starting from naphthalene is its isomerization to azulene. Solving the system of differential equations corresponding to this reaction scheme we obtained that approximately 95% of pentalene are produced immediately from azulene and 5% are formed after azulene isomerization to naphthalene and backward. This mechanism and the fact that the azulene-to-naphthalene isomerization is 2 orders of magnitude faster than the formation of pentalene from azulene make the phenylacetylene and $C_{10}H_6$ eliminations more probable reaction channels despite relatively low rate constants, although the branching ratio of 0.1% for the $C_{10}H_6$ channel seems to be too low to be observed in experiments.

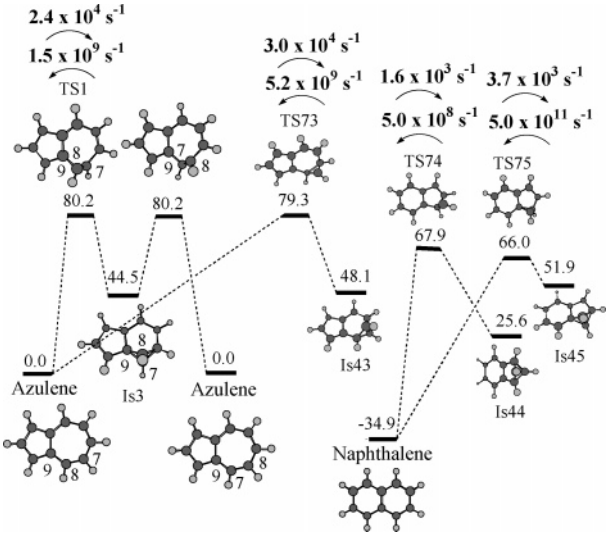

Figure 17. CH group permutations in azulene and naphthalene.

TABLE 1: Relative Energies of Azulene Photodissociation Products, Their Branching Ratios at Various Photodissociation Wavelengths, Ionization Potentials, and Adiabatic Ionization Potentials

				branching ratio, %				
product	energy, kcal/ mol	IP, eV	adiabatic IP, eV	266 nm	248 nm	193 nm	2 × 266 nm	2 × 248 nm
azulene	0.0	7.70	7.57					
naphthalene	−34.9	8.37	8.28					
P1, pentalene (+ C_2H_2)	71.7	8.00	7.64	0.0	0.0	0.7	12.4	14.0
P2, benzocyclobutadiene (+ C_2H_2)	80.1	8.06	7.47	0.0	0.0	0.0	0.3	0.4
P3, phenylacetylene (+ C_2H_2)	58.1	9.09	8.94	0.0	0.0	0.2	0.6	0.7
P4, $C_{10}H_6$ (+H_2)	66.3	8.02	7.88	0.0	0.0	0.0	0.0	0.0
P5, $C_{10}H_6$ (+H_2)	67.6	8.03	7.92	0.0	0.0	0.0	0.0	0.0
P6, $C_{10}H_6$ (+H_2)	50.0	8.69	8.64	0.0	0.0	0.1	0.8	1.0
P7, $C_{10}H_6$ (+H_2)	52.5	8.56	8.45	0.0	0.0	0.0	0.0	0.1
P8, $C_{10}H_7$ (+H)	112.8	8.48	7.10	0.0	0.0	0.0	0.1	0.1
P9, $C_{10}H_7$ (+H)	113.0	8.38	7.20	0.0	0.0	0.0	0.1	0.2
P10, $C_{10}H_7$ (+H)	114.2	8.54	7.60	0.0	0.0	0.0	0.0	0.1
P11, $C_{10}H_7$ (+H)	80.4	8.84	7.92	92.0	72.2	67.5	56.0	53.6
P12, $C_{10}H_7$ (+H)	80.8	8.76	7.86	8.0	27.8	31.5	29.7	29.8

TABLE 2: RRKM and VTST Calculated Unimolecular Rate Constants (s^{-1}), Reaction Path Degeneracies, and Barrier Heights (kcal/mol) of Various Reaction Steps in Photodissociation of Azulene at Several Values of Photon Energy

transition state	reaction	reaction path degeneracy	266 nm (107.5 kcal/mol)	248 nm (115.3 kcal/mol)	193 nm (148.1 kcal/mol)	2 × 266 nm (215.0 kcal/mol)	2 × 248 nm (230.6 kcal/mol)
TS1 + TS5 + TS6 + TS7 + TS10 + TS19	Is1 → Is2	4	4.7×10^{2}	3.1×10^{3}	7.7×10^{5}	3.4×10^{8}	9.2×10^{8}
TS1 + TS5 + TS6 + TS7 + TS10 + TS19	Is2 → Is1	8	5.3×10^{-1}	4.8×10^{0}	3.8×10^{3}	8.8×10^{6}	2.9×10^{7}
TS21	Is1 → Is17	4	1.2×10^{3}	6.8×10^{3}	1.2×10^{6}	3.2×10^{8}	6.4×10^{8}
TS21	Is17 → Is1	2	8.2×10^{7}	1.0×10^{9}	5.4×10^{9}	1.1×10^{11}	1.7×10^{11}
TS22	Is17 → P1	2	3.2×10^{1}	1.7×10^{3}	1.0×10^{7}	1.1×10^{10}	2.9×10^{10}
TS23	Is1 → Is18	4	1.4×10^{4}	6.4×10^{4}	4.5×10^{6}	9.6×10^{8}	2.0×10^{9}
TS23	Is18 → Is1	2	5.6×10^{9}	1.2×10^{10}	1.0×10^{11}	8.2×10^{11}	1.1×10^{12}
TS24	Is18 → Is19	2	6.0×10^{6}	2.4×10^{7}	8.8×10^{8}	2.6×10^{10}	4.2×10^{10}
TS24	Is19 → Is18	2	3.4×10^{7}	1.2×10^{8}	3.6×10^{9}	8.6×10^{10}	1.3×10^{11}
TS25	Is19 → P1	2	8.1×10^{3}	2.0×10^{5}	2.6×10^{8}	8.8×10^{10}	1.9×10^{11}
TS31	Is2 → Is23	8	6.0×10^{-3}	9.2×10^{-2}	2.2×10^{2}	8.8×10^{5}	3.0×10^{6}
TS31	Is23 → Is2	2	5.1×10^{9}	1.3×10^{10}	1.2×10^{11}	8.2×10^{11}	1.1×10^{12}
TS32	Is23 → Is24	2	8.3×10^{8}	3.7×10^{9}	1.2×10^{11}	2.1×10^{12}	3.1×10^{12}
TS32	Is24 → Is23	2	8.2×10^{9}	1.3×10^{10}	3.1×10^{10}	6.0×10^{10}	6.6×10^{10}
TS33	Is24 → P3	1	1.47×10^{11}	3.5×10^{11}	2.1×10^{12}	7.6×10^{12}	8.9×10^{12}
TS26	Is2 → Is20	4	8.6×10^{1}	4.4×10^{2}	6.8×10^{4}	2.4×10^{7}	6.0×10^{7}
TS26	Is20 → Is2	2	2.8×10^{9}	5.8×10^{9}	4.7×10^{10}	4.0×10^{11}	5.6×10^{11}
TS28	Is20 → Is22	4	5.2×10^{2}	1.1×10^{4}	1.5×10^{7}	8.4×10^{9}	2.0×10^{10}
TS28	Is22 → Is20	2	2.0×10^{10}	4.9×10^{10}	3.0×10^{11}	1.0×10^{12}	1.2×10^{12}
TS30	Is22 → P2	2	2.7×10^{7}	5.2×10^{8}	7.3×10^{10}	1.6×10^{12}	2.3×10^{12}
TS29	Is21 → Is22	2	7.2×10^{6}	5.4×10^{7}	5.9×10^{9}	2.4×10^{11}	4.0×10^{11}
TS29	Is22 → Is21	2	1.6×10^{10}	3.7×10^{10}	1.9×10^{11}	5.8×10^{11}	6.7×10^{11}
TS27	Is2 → Is21	8	4.6×10^{-8}	6.7×10^{-6}	9.6×10^{-1}	5.5×10^{3}	2.7×10^{5}
TS27	Is21 → Is2	2	2.3×10^{4}	5.8×10^{5}	4.0×10^{8}	5.1×10^{10}	9.6×10^{10}
VTST	Is2 → P12	4	2.5×10^{-2}	4.9×10^{-1}	5.4×10^{3}	4.3×10^{6}	1.4×10^{7}
VTST	Is2 → P11	4	2.0×10^{-2}	4.0×10^{-1}	5.6×10^{3}	4.5×10^{6}	1.5×10^{7}
TS65 + TS66 + TS60 + TS61	Is2 → P11	8	1.3×10^{1}	4.5×10^{1}	3.6×10^{4}	6.0×10^{7}	1.8×10^{8}
TS54 + TS55 + TS48 + TS49 + TS16	Is2 → P12	8	$1.1 \times 10^{\circ}$	1.7×10^{1}	1.4×10^{4}	3.0×10^{7}	9.5×10^{7}
TS41 + TS43	Is2 → P6	4	4.8×10^{-4}	1.8×10^{-2}	6.2×10^{1}	8.8×10^{5}	3.5×10^{6}
TS45	Is2 → P7	4	8.8×10^{-6}	3.5×10^{-4}	6.2×10^{0}	1.1×10^{5}	4.5×10^{5}
VTST	Is1 → P8 + P9 + P10	5	-	1.3×10^{-8}	1.8×10^{0}	6.05×10^{5}	3.2×10^{6}
TS36 + TS37	Is1 → P4	2	-	2.8×10^{-11}	3.9×10^{-2}	2.6×10^{4}	1.5×10^{5}
TS38 + TS39	Is1 → P5	2	-	3.5×10^{-10}	4.6×10^{-1}	1.3×10^{4}	1.5×10^{5}

The most recent molecular beam experiment[36] that revealed a small yield of C_8H_6 fragments points to pentalene elimination rather than phenylacetylene due to too high reverse barrier for the phenylacetylene elimination reaction and higher ionization potential (IP) of phenylacetylene. In fact, C_8H_6 fragments were observed even at the energy of ionization photons as low as 7.9 eV (157 nm), whereas calculated IP for phenylacetylene is 9.1 eV, as seen in Table 1. The calculated IP for pentalene is 8.0 eV, which is close to the experimental energy of ionization photons, 7.9 eV.

Concluding the discussion about the reaction pathways and rate constants, let us consider the possibility of CH-group exchange reactions in the seven-member ring of azulene and six-member rings of naphthalene. Figure 17 presents the scheme and rate constants for these processes. For these rate constant calculations, we supposed that one of the carbon atoms was substituted by the ^{13}C isotope, which decreased the symmetry of the system. Rate constants for the forward direction divided by a factor of 2 give approximate rate constants for the isotope exchange reaction if one of the carbons is replaced by the ^{13}C

isotope. The factor of 2 arises because after rearrangement into benzvalene-like intermediate (**Is3**, **Is43**, **Is44**, and **Is45** in Figure 17) only a half of the molecules will proceed to the isotope-shifted isomer, the other half will return to the initial configuration. The ratio of the rate constant for the isotope-exchange reaction in azulene and the rate constant for azulene-to-naphthalene isomerization gives the relative amount of azulene molecules which change their isotope labeled carbon positions before rearrangement to naphthalene. For the routes through **TS1** and **TS73,** calculations give the branching ratios of 1.5% and 1.9%, respectively. Employing the same procedure to naphthalene, we obtain that 1.3% and 3.0% (for the routes through **TS74** and **TS75**, respectively) of isotope labeled carbons will change their position before dissociation. Analyzing these data, we can conclude that isotope exchange processes in azulene and naphthalene do not play an important role in the azulene photodissociation reaction. So, the isotope exchange observed in experiment is mostly due to various mechanisms of azulene-to-naphthalene isomerization described above.

To predict possible outcomes of future photodissociation experiments at different wavelengths, we additionally calculated rate constants and product yields upon absorption of one or two 266 and 248 nm photons. The results are summarized in Table 1 (branching ratios) and Table 2 (rate constants). According to our results, the yield of pentalene strongly depends on the photon energy, and grows from 0% at 266 and 248 nm to 14% at the 2×248 nm excitation. The yield of H_2 molecules from naphthalene could be observed only at 2×266 and 2×248 excitations. With the energy increase, it grows from 0% at 266 nm to 1.1% upon absorption of two 248 nm photons. The branching ratio of the benzocyclobutadiene channel also rises with the photoexcitation wavelength and becomes 0.4% when two 248 nm photons are absorbed. The calculated yield of phenylacetylene increases from 0% at 266 nm to 0.7% at $2 \times$ 248 nm and then remains nearly unchanged at higher excitation energies. H-atom elimination remains the dominant photodissociation channel at all excitation wavelengths studied; however, the yield of H-atoms steadily decreases with the increasing photon energy, from 100% at 266 nm to 83.7% at 2×248 nm.

Conclusions

High-level ab initio calculations of various mechanisms of isomerization of neutral azulene to naphthalene following photoexcitation by 193 nm photons and fast internal conversion into the vibrationally excited ground electronic state show that the dominant reaction pathway is the one-step norcaradiene−vinylidene (Dewar−Becker) mechanism, in which the rearrangement of two carbon rings and a hydrogen shift occur in a concerted manner. The calculated barrier for this pathway is 72.4 kcal/mol. The other considered mechanisms exhibit notably higher barriers and play minor roles; their contribution to the overall yield of naphthalene from azulene amounts to about 7%. The overall rate constant of the azulene-to-naphthalene rearrangement calculated for the available internal energy of 148.1 kcal/mol (193 nm) is 7.7×10^5 s^{-1}, in close agreement with the experimentally measured value of 4.1×10^5 s^{-1}. Once naphthalene is formed from azulene (under collissionless molecular beam conditions), it can decompose mostly through elimination of a hydrogen atom giving α- and β-naphthyl as 31.7% and 68.0% of the total products, respectively. Direct dissociation of azulene without isomerization to naphthalene is much less likely because of unfavorable energetics and very low rate constants.

In addition to the H elimination channels, which give 99% of the total product yield at 193 nm, minor decomposition channels include pentalene + C_2H_2 (0.7%), phenylacetylene + C_2H_2 (0.2%), and a trace amount of $C_{10}H_6 + H_2$ (0.1%). The pentalene + acetylene products can be formed directly from azulene (95%), where this process will, to some extent, compete with the isomerization to naphthalene, or after the rearrangement to naphthalene and backward to azulene (5%). The other fragments are produced from naphthalene. Among different possible C_8H_6 products formed by acetylene elimination, benzocyclobutadiene is very unlikely to be observed at the 6.4 eV excitation energy due to a high dissociation barrier as compared to the other dissociation pathways. Therefore, the C_8H_6 molecules detected experimentally upon photodissociation of azulene at 193 nm are probably only pentalene and phenylacetylene. A comparison of the calculated product branching ratios at different excitation energies shows that the ratio between pentalene and phenylacetylene strongly depends on the excitation energy, and the yield of pentalene rapidly grows with the energy increase, whereas the amount of phenylacetylene remains small. The yield of H-atoms decreases in favor of acetylene with an increase of the photon energy, but $C_{10}H_7$ + H remain the most important photodissociation products (83.7%) even upon absorption of two 248 nm photons.

Acknowledgment. This work was supported in part by Academia Sinica and the National Science Council of Taiwan, R.O.C., at IAMS, and by the Chemical Sciences, Geosciences and Biosciences Division, Office of Basic Energy Sciences, Office of Sciences of the U.S. Department of Energy (Grant No. DE-FG02-04ER15570) at FIU.

Supporting Information Available: Optimized Cartesian coordinates of all species involved in the azulene isomerization and dissociation reactions and their total energies including ZPE calculated at the B3LYP/6-31G* level of theory. This material is available free of charge via the Internet at http://pubs.acs.org.

References and Notes

(1) Leger, A.; Puget, J.-L. *Astron. Astrophys.* **1984**, *137*, L5-L8.
(2) Allamandola, L. J.; Tielens, A. G. G. M.; Barker, J. R. *Astrophys. J.* **1985**, *290*, L25-L28.
(3) Heilbronner, E.; Wieland, K. *Helv. Chim. Acta* **1947**, *30*, 947.
(4) Scott, L. T.; Agopian, G. K. *J. Am. Chem. Soc.* **1977**, *99*, 4506.
(5) Alder, R. W.; Whittaker, G. *J. Chem. Soc., Perkin Trans.* 2 **1975**, 714.
(6) Alder, R. W.; Wilshire, C. *J. Chem. Soc., Perkin Trans.* 2 **1975**, 1464.
(7) Alder, R. W.; Whiteside, R. W.; Whittaker, G.; Wilshire, C. *J. Am. Chem. Soc.* **1979**, *101*, 629.
(8) Becker, J.; Wentrup, C.; Katz, E.; Zeller, K.-P. *J. Am. Chem. Soc.* **1980**, *102*, 5112.
(9) Scott, L. T.; Kirms, M. A. *J. Am. Chem. Soc.* **1981**, *103*, 5875.
(10) Gugel, H.; Zeller, K.-P.; Wentrup, C. *Chem. Ber.* **1983**, *116*, 2775.
(11) Scott, L. T.; Kirms, M. A.; Earl, B. L. *J. Chem. Soc., Chem. Commun.* **1983**, 1373.
(12) Wetzel, A.; Zeller, K.-P. *Z. Naturforsch. B* **1987**, *42*, 903.
(13) Brouwer, L.; Troe, J. *Int. J. Chem. Kinet.* **1988**, *20*, 379.
(14) Laskin, A.; Lifshitz, A. *Isr. J. Chem.* **1996**, *36*, 257.
(15) Keller, F.; Beckhaus, H.-D.; Rüchardt, C. *Liebigs Ann. Recl.* **1997**, 2055.
(16) Scott, L. T. *Acc. Chem. Res.* **1982**, *15*, 52.
(17) Scott, L. T. *J. Org. Chem.*, **1984**, *49*, 3021.
(18) Dewar, M. J. S.; Merz, K. M. *J. Am. Chem. Soc.* **1985**, *107*, 6111.
(19) Dewar, M. J. S.; Merz, K. M. *J. Am. Chem. Soc.* **1986**, *108*, 5142.
(20) Dewar, M. J. S.; Merz, K. M. *J. Am. Chem. Soc.* **1986**, *108*, 5146.
(21) Alder, R. W.; East, S. P.; Harvey, J. N.; Oakley, M. T. *J. Am. Chem. Soc.* **2003**, *125*, 5375.
(22) Stirling, A.; Iannuzzi, M.; Liao, A.; Parrinello, M. *ChemPhysChem.* **2004**, *5*, 1558.
(23) Jochims, H. W.; Rasekh, H.; Rühl, E.; Baumgärtel, H.; Leach, S. *Chem. Phys.* **1992**, *168*, 159.
(24) Jochims, H. W.; Rasekh, H.; Rühl, E.; Baumgärtel, H.; Leach, S. *J. Phys. Chem.* **1993**, *97*, 1312.

(25) Gotkis, Y.; Oleinikova, M.; Naor, M.; Lifshitz, C. *J. Phys. Chem.* **1993**, *97*, 12282.

(26) Ling, Y.; Martin, J. M. L.; Lifshitz, C. *J. Phys. Chem. A*, **1997**, *101*, 219.

(27) Ling, Y.; Lifshitz, C. *J. Phys. Chem. A*, **1998**, *102*, 708.

(28) Koster, G.; Martin, J. M. L.; Lifshitz, C. *J. Chem. Soc., Perkin Trans. 2* **1999**, 2383.

(29) Cui, W.; Hadas, B.; Cao, B.; Lifshitz, C. *J. Phys. Chem. A* **2000**, *104*, 6339.

(30) Schroeter, K.; Schröder, D.; Schwarz, H. *J. Phys. Chem. A* **1999**, *103*, 4174.

(31) van der Hart, W. J. *Int. J. Mass Spectrom.* **2002**, *214*, 269.

(32) Damm, M.; Hippler, H.; Troe, J. *J. Chem. Phys.* **1988**, *88*, 3564.

(33) Damm, M.; Deckert, F.; Hippler, H.; Troe, J. *J. Phys. Chem.* **1991**, *95*, 2005.

(34) Diau, E. W.-G.; Feyter, S. D.; Zewail, A. H. *J. Chem. Phys*. **1999**, *110*, 9785.

(35) Lin, M. F.; Huang, C. L.; Lee, Y. T.; Ni, C. K. *J. Chem. Phys*. **2003**, *119*, 2032.

(36) Tseng, C. M.; Lin, M. F.; Dyakov, Y. A.; Lee, Y. T.; Ni, C. K. To be submitted for publication.

(37) (a) Becke, A. D. *J. Chem. Phys*. **1992**, *96*, 2155. (b) Becke, A. D. *J. Chem. Phys*. **1992**, *97*, 9173. (c) Becke, A. D. *J. Chem. Phys*. **1993**, *98*, 5648.

(38) Lee, C.; Yang, W.; Parr, R. G. *Phys. Rev*. **1988**, *B37*, 785.

(39) Hehre, W. J.; Ditchfield, R.; Pople, J. A. *J. Chem. Phys.* **1972**, *56*, 2257.

(40) (a) Curtiss, L. A.; Raghavachari, K.; Redfern, P. C.; Rassolov, V.; Pople, J. A. *J. Chem. Phys.* **1998**, *109*, 7764. (b) Baboul, A. G.; Curtiss, L. A.; Redfern, P. C.; Raghavachari, K. *J. Chem. Phys.* **1999**, *110*, 7650. (c) Curtiss, L. A.; Raghavachari, K.; Redfern, P. C.; Baboul, A. G.; Pople, J. A. *Chem. Phys. Lett.* **1999**, *314*, 101.

(41) Frisch, M. J.; Trucks, G. W.; Schlegel, H. B.; Scuseria, G. E.; Robb, M. A.; Cheeseman, J. R.; Zakrzewski, V. G.; Montgomery, J. A., Jr.; Stratmann, R. E.; Burant, J. C.; Dapprich, S.; Millam, J. M.; Daniels, A. D.; Kudin, K. N.; Strain, M. C.; Farkas, O.; Tomasi, J.; Barone, V.; Cossi, M.; Cammi, R.; Mennucci, B.; Pomelli, C.; Adamo, C.; Clifford, S.; Ochterski, J.; Petersson, G. A.; Ayala, P. Y.; Cui, Q.; Morokuma, K.; Malick, D. K.; Rabuck, A. D.; Raghavachari, K.; Foresman, J. B.; Cioslowski, J.; Ortiz, J. V.; Stefanov, B. B.; Liu, G.; Liashenko, A.; Piskorz, P.; Komaromi, I.; Gomperts, R.; Martin, R. L.; Fox, D. J.; Keith, T.; Al-Laham, M. A.; Peng, C. Y.; Nanayakkara, A.; Gonzalez, C.; Challacombe, M.; Gill, P. M. W.; Johnson, B.; Chen, W.; Wong, M. W.; Andres, J. L.; Gonzalez, C.; Head-Gordon, M.; Replogle, E. S.; Pople, J. A. *Gaussian 9*8, revision A.7; Gaussian, Inc.: Pittsburgh, PA, 1998.

(42) MOLPRO is a package of ab initio programs written by H.-J. Werner and P. J. Knowles with contributions from Almlöf, J.; Amos, R. D.; Deegan, M. J. O.; Elbert, S. T.; Hampel, C.; Meyer, W.; Peterson, K.; Pitzer, R.; Stone, A. J.; Taylor, P. R.; and Lindh, R.

(43) Eyring, H.; Lin, S. H.; Lin, S. M. *Basic Chemical Kinetics*; Wiley: New York, 1980.

(44) Robinson P. J.; Holbrook, K. A. *Unimolecular Reactions*; Wiley: New York, 1972.

(45) Steinfeld, J. I.; Francisco, J. S.; Hase, W. L. *Chemical Kinetics and Dynamics*; Prentice Hall: Upper Saddle River, NJ, 1999).

(46) Kislov, V. V.; Nguyen T. L.; Mebel, A. M.; Lin, S. H.; Smith, S. C. *J. Chem. Phys.* **2004**, *120*, 7008.